Two-dimensional dispersion entropy: an information-theoretic method for irregularity analysis of images

Hamed Azami, L.E.V. da Silva, A.C.M. Omoto, Anne Humeau-Heurtier

Version of Record: https://www.sciencedirect.com/science/article/pii/S0923596519300682
Manuscript_9327dab9f663c5fdaaf251847648ffc1

Two-dimensional dispersion entropy: an information-theoretic method for irregularity analysis of images

Hamed Azami[a], Luiz Eduardo Virgilio da Silva[b], Ana Carolina Mieko Omoto[b], Anne Humeau-Heurtier[c,*]

[a] *Department of Neurology and Massachusetts General Hospital, Harvard University, Boston, USA*
[b] *Department of Physiology, School of Medicine of Ribeirao Preto, University of Sao Paulo, Ribeirao Preto, SP, Brazil*
[c] *Univ Angers, LARIS - Laboratoire Angevin de Recherche en Ingénierie des Systèmes, 62 avenue Notre-Dame du Lac, 49000 Angers, France*

Abstract

Two-dimensional sample entropy (SampEn_{2D}) is a recently developed method in the field of information theory for evaluating the regularity or predictability of images. SampEn_{2D}, though powerful, has two key limitations: 1) SampEn_{2D} values are undefined for small-sized images; and 2) SampEn_{2D} is computationally expensive for several real-world applications. To overcome these drawbacks, we introduce the two-dimensional dispersion entropy (DispEn_{2D}) measure. To evaluate the ability of DispEn_{2D}, in comparison with SampEn_{2D}, we use various synthetic and real datasets. The results demonstrate that DispEn_{2D} distinguishes different amounts of white Gaussian and salt and pepper noise. The periodic images, compared with their corresponding synthesized ones, have lower DispEn_{2D} values. The results for Kylberg texture dataset show the ability of DispEn_{2D} to differentiate various textures. Although the results based on DispEn_{2D} and SampEn_{2D} for both the synthetic and real datasets are consistent in that they lead to similar findings about the irregularity of images, DispEn_{2D} has three main advantages over SampEn_{2D}: 1) DispEn_{2D}, unlike SampEn_{2D}, does not lead to undefined values; 2) DispEn_{2D} is noticeably quicker; and 3) The coeffi-

*Corresponding author:
Email address: anne.humeau@univ-angers.fr (Anne Humeau-Heurtier)

cient of variations and Mann-Whitney U test-based p-values for $\text{DispEn}_{2\text{D}}$ are considerably smaller, showing the more stability of the $\text{DispEn}_{2\text{D}}$ results. Overall, thanks to its successful performance and low computational time, $\text{DispEn}_{2\text{D}}$ opens up a new way to analyze the uncertainty of images.

Keywords:
Biomedical image processing, texture analysis, irregularity, two-dimensional dispersion entropy, two-dimensional sample entropy

---

1. Introduction

In the field of signal and image processing, information theory provides tools for information representation and manipulation [1, 2]. Entropy, as a prominent concept in information theory, is a measure of the uncertainty or irregularity of a system or data [2, 3]. Following the concept of entropy introduced by Shannon, several methods, such as one-dimensional approximate entropy ($\text{ApEn}_{1\text{D}}$) [4], sample entropy ($\text{SampEn}_{1\text{D}}$) [3], permutation entropy ($\text{PerEn}_{1\text{D}}$) [5], distribution entropy ($\text{DistrEn}_{1\text{D}}$) [6], and dispersion entropy ($\text{DispEn}_{1\text{D}}$) [7] have been introduced.

$\text{ApEn}_{1\text{D}}$ was proposed in 1991 to estimate the irregularity of time series [4]. $\text{ApEn}_{1\text{D}}$ is based on the negative average natural logarithm of the conditional probability that two sequences that are similar for m points remain similar, within a tolerance r, at the next point. $\text{SampEn}_{1\text{D}}$ overcomes the problem of counting self-similar patterns in $\text{ApEn}_{1\text{D}}$, leading to more reliable estimations [3]. $\text{SampEn}_{1\text{D}}$ has been widely employed in many biomedical signal processing applications [8, 9, 10, 11].

Nevertheless, $\text{SampEn}_{1\text{D}}$ is not fast enough for long time series and its values may be undefined for short signals [7]. $\text{PerEn}_{1\text{D}}$ is on the basis of permutations defined by the order relations among values of a signal [5]. $\text{PerEn}_{1\text{D}}$ has been broadly used in many signal processing analyses and cognitive neuroscience studies to detect different dynamics of various signals [12]. $\text{PerEn}_{1\text{D}}$ is computationally fast (computation cost of $\text{O}(N)$) [26]. Nevertheless, it has three key deficiencies: i) when a time series is symbolized based on its permutation patterns, only the order of the amplitude values is considered and some information about the amplitude values is ignored [12, 13], ii) the effect of equal amplitude values in each embedding vector was not addressed in PerEn [12, 13]; and iii) the most important shortcoming of PerEn is its high sensitivity to noise. This occurs because a small change in amplitude

value may vary the order relations among amplitudes [13], even when the signal-to-noise ratio (SNR) of a signal is high (for more information, please see Figure 9 in [13]).

To overcome the shortcomings of PerEn_{1D} and SampEn_{1D}, DispEn_{1D} has been very recently introduced as a fast and powerful technique to quantify the irregularity of signals [7]. The dependency of DispEn_{1D} on a number of straightforward signal processing concepts via a set of synthetic time series and three real publicly-available datasets was previously evaluated. The results showed that the DispEn_{1D} technique noticeably outperforms PerEn_{1D} in terms of detection of dynamics of signals [7]. Also, the results demonstrated that DispEn_{1D} is sensitive to changes in frequency, simultaneous amplitude and frequency, noise power, and noise bandwidth. Moreover, the computational time for DispEn_{1D} is considerably lower than that for SampEn_{1D} [7]. It was also found that DispEn_{1D}, compared with PerEn_{1D} and SampEn_{1D}, is the most consistent technique to discriminate young from elderly children's stride-to-stride recordings, and the salt-sensitive from salt protected rats' blood pressure data [13].

Some of the above-mentioned entropy measures for the analysis of signals have recently been extended to their corresponding bi-dimensional cases to process images. Thus, multi-dimensional ApEn was introduced and applied to the biomedical field [18, 19, 20]. Two-dimensional SampEn (SampEn_{2D}), as an extension of SampEn_{1D}, has been recently proposed to take into account the predictability of patterns within images [21, 22]. It has been demonstrated that SampEn_{2D}, as a powerful tool for the feature extraction of images, follows SampEn_{1D} for different straight-forward concepts in signal and image processing such as noise, nonlinearity, and randomness, and can be considered as an irregularity measure of images [22]. Another advantage of SampEn_{2D} is its invariance to rotation and translation [22]. Moreover, two-dimensional PerEn (PerEn_{2D}) was also proposed as an extension of its one-dimensional entropy counterpart [23, 24, 25]. Thus, a generalization of the complexity-entropy causality plane to 2D maps was developed. PerEn_{2D} was able to detect different kinds of two-dimensional patterns [23].

To take advantages of the performance of DispEn_{1D} over SampEn_{1D} and PerEn_{1D} [7], we introduce here two-dimensional DispEn (DispEn_{2D}), as an extension of DispEn_{1D}. In this paper, we evaluate DispEn_{2D} on synthetic images and Brodatz and Kylberg publicly-available texture datasets, as well as on a real dataset of histological cardiac images. We show that the main advantages of the proposed DispEn_{2D} are: i) DispEn_{2D}, unlike

SampEn_{2D}, does not result in undefined values for small images; ii) DispEn_{2D} is noticeably faster than SampEn_{2D}; and iii) DispEn_{2D} leads to more stable results than SampEn_{2D}.

We have very recently introduced the bi-dimensional version of the distribution entropy (DistrEn_{2D}) [27]. In spite of its interesting results, we will not compare DispEn_{2D} with DistrEn_{2D} because DistrEn_{2D} is interesting mainly for small-sized textures [27], whereas DispEn_{2D} can take into account both small and large images. Furthermore, randomly shuffling an image does not change considerably the value of DistrEn_{2D}. However, the correlations among the image pixels are destroyed in shuffles, and the irregularity of the image surrogates should be higher than that of the original image (except 2-D random images). Moreover, due to the drawbacks of PerEn_{1D} mentioned above, we do not compare DispEn_{2D} with PerEn_{2D}. DispEn_{2D} is also not compared to the bi-dimensional version of multiscale SampEn_{2D} [28] as the latter relies on a multiscale approach and is therefore a measure of image complexity, whereas DispEn_{2D} is a single-scale approach.

The remaining of the paper is organized as follows. Section 2 details DispEn_{1D} and SampEn_{2D}. The datasets used to evaluate DispEn_{2D} are described in Section 3. In Section 4, the results for DispEn_{2D}, in comparison of SampEn_{2D}, are shown and discussed. We finally end with a conclusion.

2. Two-dimensional Dispersion Entropy and Sample Entropy Measures

2.1. The Proposed Algorithm: Two-dimensional Dispersion Entropy

DispEn_{2D} is an extension of DispEn_{1D} for two-dimensional data. Assume we have an image of size $h \times w$: $\mathbf{U} = \{u_{i,j}\}_{i=1,2,\dots,h}^{j=1,2,\dots,w}$, defined on a domain $\mathbb{R}^2$. DispEn_{2D} of $\mathbf{U}$ is defined as follows:

1) First, $u_{i,j}$ are mapped to c classes with integer indices from 1 to c. To this aim, there are a number of linear and nonlinear mapping approaches used in the DispEn-based methods [13]. Some linear and nonlinear algorithms can be used to map the original image to the classified image. The simplest and fastest algorithm is the linear mapping. However, when maximum or minimum values are noticeably larger or smaller than the mean/median value of the signal, the majority of values are mapped to only a few classes [13]. On the other hand, a large number of natural processes show a progression from

small beginnings that accelerates and approaches a climax over time (e.g., a sigmoid function) [14, 15]. When there is not a detailed description, a sigmoid function is frequently used [16, 15, 17]. Thus, we take the normal cumulative distribution function (NCDF) of pixels to map the image into the classes, as this function naturally raises in a sigmoidal shape. NCDF maps $\mathbf{U}$ into $\mathbf{Y} = \{y_{i,j}\}_{i=1,2,\dots,h}^{j=1,2,\dots,w}$ from 0 to 1 as follows

$$y_{i,j} = \frac{1}{\sigma\sqrt{2\pi}} \int_{-\infty}^{x_{i,j}} e^{\frac{-(t-\mu)^2}{2\sigma^2}} \, \mathrm{d}t, \tag{1}$$

where μ and σ are the average and standard deviation of $\mathbf{U}$, respectively. Next, we use a linear algorithm to assign each $y_{i,j}$ to an integer from 1 to c. To this end, for each $x_{i,j}$, we use $z_{i,j}^c = \text{round}(c \times y_{i,j} + 0.5)$, where $z_{i,j}^c$ shows the $(i,j)^{th}$ pixel of the classified image and rounding involves either increasing or decreasing a number to the next digit.

2) $\mathbf{z}_{k,l}^{\mathbf{m},c}$ are made with the embedding dimension vector $\mathbf{m} = [m_h, m_w]$ according to

$$\begin{aligned} \mathbf{z}_{k,l}^{\mathbf{m},c} = \{ & z_{k,l}^c, z_{k,l+1}^c, ..., z_{k,l+(m_w-1)}^c, \\ & z_{k+1,l}^c, z_{k+1,l+1}^c, ..., z_{k+1,l+(m_w-1)}^c, ..., \\ & z_{k+(m_h-1),l}^c, z_{k+(m_h-1),l+1}^c, ..., z_{k+(m_h-1),l+(m_w-1)}^c \}, \end{aligned} \tag{2}$$

where $k = 1, 2, \dots, w - (m_w - 1)$ and $l = 1, 2, \dots, h - (m_h - 1)$. Each matrix $\mathbf{z}_{k,l}^{m,c}$ is mapped to a dispersion pattern $\pi_{v_0 v_1 \dots v_{m_h \times m_w - 1}}$, where $z_{k,l}^c = v_0$, $z_{k,l+1}^c = v_1, \dots, \ z_{k+(m_h-1),l+(m_w-1)}^c = v_{m_h \times m_w - 1}$. The number of possible dispersion patterns that can be assigned to each matrix $\mathbf{z}_{k,l}^{\mathbf{m},c}$ is equal to $c^{m_h \times m_w}$, since the matrix $\mathbf{z}$ has $m_h \times m_w$ members and each member can be one of the integers from 1 to c [7].

3) For each $c^{m_h \times m_w}$ potential dispersion patterns $\pi_{v_0 \dots v_{m_h \times m_w - 1}}$, relative frequency is obtained as follows

$$p(\pi_{v_0 \dots v_{m_h \times m_w - 1}}) = \frac{\#\{k, l \,\big|\, \begin{matrix} k \le h - (m_h - 1) \\ l \le w - (m_w - 1) \end{matrix}, \mathbf{z}_{k,l}^{\mathbf{m},c} \text{ has type } \pi_{v_0 \dots v_{m_h . m_w - 1}} \}}{(h - (m_h - 1))(w - (m_w - 1))}. \tag{3}$$

In fact, $p(\pi_{v_0 \dots v_{m_h . m_w - 1}})$ shows the number of dispersion patterns of $\pi_{v_0 \dots v_{m_h . m_w - 1}}$ that is assigned to $\mathbf{z}_{k,l}^{\mathbf{m},c}$, divided by the total number of embedded vectors with embedding dimension $\mathbf{m}$.

4) Finally, based on Shannon's definition of entropy, $\mathrm{DispEn_{2D}}$ is computed as follows

$$DispEn_{2D}(\mathbf{U}, \mathbf{m}, c) = \\ -\sum_{\pi=1}^{c^{m_w \times m_h}} p(\pi_{v_0 \ldots v_{m_w \times m_h - 1}}) \times \ln\left(p(\pi_{v_0 \ldots v_{m_w \times m_h - 1}})\right). \tag{4}$$

When all possible two-dimensional dispersion patterns of an image have equal probability value, the highest value of $\mathrm{DispEn_{2D}}$ is reached, which has a value of $\ln(c^{m_h \times m_w})$. However, if there is only one $p(\pi_{v_0 \ldots v_{m_h \times m_w - 1}})$ different from zero, showing a completely regular and certain image, the smallest value of $\mathrm{DispEn_{2D}}$ is obtained.

As for $\mathrm{DispEn_{1D}}$ [7], the number of classes for $\mathrm{DispEn_{2D}}$ can be chosen from 3 to 9. The number of classes (c) in DispEn algorithms is inversely related to the threshold value r used in the SampEn approaches [13]. Thus, when the signal-to-noise ratio (SNR) is high, it is recommended to choose a large value of c, while a small c is more appropriate for signals with low SNR. Nevertheless, for convenience, we can set $c = 5$ for all images according to [7]. To work with reliable statistics to calculate $\mathrm{DispEn_{2D}}$, it is recommended that the number of potential patterns ($c^{m_h \times m_w}$) is smaller than the number of patterns of an image ($(h - (m_h - 1)) \times (w - (m_w - 1))$).

2.2. Two-dimensional Sample Entropy

Assume an image of size $h \times w$: $\mathbf{U} = \{u_{i,j}\}_{i=1,2,\ldots,h}^{j=1,2,\ldots,w}$, defined on a domain $\mathbb{R}^2$. To compute $\mathrm{SampEn_{2D}}$, first all two-dimensional matrices $\mathbf{X}_{k,l}^{\mathbf{m}}$ ($k = 1, 2, ..., h - (m_h - 1)$ and $l = 1, 2, ..., w - (m_w - 1)$) with size $m_h \times m_w$, named template matrices, are created as

$$\mathbf{X}_{k,l}^{\mathbf{m}} = \begin{bmatrix} u_{k,l} & u_{k,l+1} & \cdots & u_{k,l+(m_w-1)} \\ u_{k+1,l} & u_{k+1,l+1} & \cdots & u_{k+1,l+(m_w-1)} \\ \vdots & \vdots & \vdots & \vdots \\ u_{k+(m_h-1),l} & u_{k+(m_h-1),l+1} & \cdots & u_{k+(m_h-1),l+(m_w-1)} \end{bmatrix}, \tag{5}$$

where $\mathbf{m} = [m_h, m_w]$ is the embedding dimension vector [22].

Then, the number of element pairs in template matrices of size $m_h \times m_w$ having $d[\mathbf{X}_{k,l}^{\mathbf{m}}, \mathbf{X}_{a,b}^{\mathbf{m}}] \leq r$ is computed as

$$\phi^{\mathbf{m}}_{k,l}(r) = \frac{[\#\ of\ \mathbf{X}^{\mathbf{m}}_{a,b} \mid d[\ \mathbf{X}^{\mathbf{m}}_{k,l}, \mathbf{X}^{\mathbf{m}}_{a,b}] \leq r]}{(h-m_h)(w-m_w)-1}, \tag{6}$$

where a and b respectively change from 1 to $h-m_h$ and $w-m_w$ ($(a,b) \neq (k,l)$), $d[\mathbf{X}^{\mathbf{m}}_{k,l}, \mathbf{X}^{\mathbf{m}}_{a,b}]$ denotes the greatest element of the absolute differences between $\mathbf{X}^{\mathbf{m}}_{k,l}$ and $\mathbf{X}^{\mathbf{m}}_{a,b}$, and r is the predefined threshold (tolerance factor) [22].
Next, $\phi^{\mathbf{m}}(r)$ is calculated as

$$\phi^{\mathbf{m}}(r) = \frac{1}{(h-m_h)(w-m_w)} \sum_{k=1}^{k=h-m_h} \sum_{l=1}^{l=w-m_w} \phi^{\mathbf{m}}_{k,l}(r). \tag{7}$$

Then, $\phi^{\mathbf{m}+1}(r)$ is computed in the same way, increasing $\mathbf{m}$ to $\mathbf{m}+1$ where $\mathbf{m}+1 = [m_h+1, m_w+1]$ and $\phi^{\mathbf{m}+1}_{k,l}(r)$ is as follows

$$\phi^{\mathbf{m}+1}_{k,l}(r) = \frac{[\#\ of\ \mathbf{X}^{\mathbf{m}+1}_{a,b} \mid d[\ \mathbf{X}^{\mathbf{m}+1}_{k,l}, \mathbf{X}^{\mathbf{m}+1}_{a,b}] \leq r]}{(h-m_h)(w-m_w)-1}. \tag{8}$$

Finally, $\text{SampEn}_{2\text{D}}$ is defined as follows [22]

$$SampEn_{2D}(\mathbf{U}, \mathbf{m}, r) = -\ln \frac{\phi^{\mathbf{m}+1}(r)}{\phi^{\mathbf{m}}(r)}. \tag{9}$$

The parameter $\mathbf{m}$ indicates the size of the matrices which are analyzed or compared along images. In previous studies [22, 21], $\mathbf{m}$ was chosen to obtain squared template matrices, i.e. $m_h = m_w$.

The parameter r is chosen to balance the quality of the logarithmic likelihood estimates with the loss of signals' or images' information. When r is too small (smaller than 0.1 of the standard deviation of an image), poor conditional probability estimates are achieved. Furthermore, to avoid the effect of noise on data, larger r is recommended. In contrast, for r values larger than 0.4 of the standard deviation, too much detailed data information is lost. Therefore, a trade-off between large and small r values is needed. For a deeper discussion on the effect of those parameters in $\text{SampEn}_{2\text{D}}$, please refer to [22].

Figure 1: Example of a reference image, sized 256×256 pixels, on which different levels of $\mathrm{WGN_{2D}}$ and $\mathrm{SPN_{2D}}$ were added.

3. Synthetic and Real Image Datasets

In this section, the synthetic and real images used to evaluate the performance of $\mathrm{DispEn_{2D}}$ are described.

3.1. Synthetic Datasets

3.1.1. Texture Image with Additive Noise

To evaluate the dependency of $\mathrm{DispEn_{2D}}$ on two-dimensional white Gaussian noise ($\mathrm{WGN_{2D}}$) and salt and pepper noise ($\mathrm{SPN_{2D}}$; sparsely occurring white and black pixels), we employed Lenna as a standard widely-used image, sized 256×256 pixels, shown in Figure 1. After normalizing the image in the range 0 to 1, we added different levels of uniform $\mathrm{WGN_{2D}}$ with mean (variance) equals to 0.01 (0.01), 0.05 (0.05), and 0.09 (0.09). We also added $\mathrm{SPN_{2D}}$ with different noise density values of 0.01, 0.05, and 0.09 to the reference normalized image.

3.1.2. Artificial Periodic and Synthesized Textures

To show how $\mathrm{DispEn_{2D}}$ changes when a periodic texture image turns into its synthesized one, we used four pairs of periodic and their corresponding synthesized textures from [29]. The original and their synthesized textures, sized 256×256 pixels, are depicted in Figure 2(a) to (d), and Figure 2(e) to (h), in that order. The synthesis algorithm, which is based on Markov random field texture models, generated textures through a deterministic search process [30]. Note that each local region of the synthesized texture based on this algorithm is similar to another region from the input (original periodic) texture.

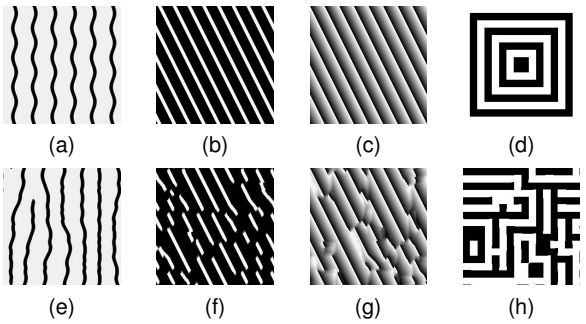

Figure 2: Texture synthesis examples: (a), (b), (c), and (d) periodic textures and (e), (f), (g), and (h) their corresponding synthesized textures [29]. All images have a size of 256×256 pixels.

3.1.3. Two-dimensional MIX Process (MIX_{2D})

We also compare the performance of $\mathrm{DispEn_{2D}}$ and $\mathrm{SampEn_{2D}}$ using the MIX processes. For the one-dimensional case, MIX(p) is a family of processes that interleave samples of a sine wave and sample of independent identically distributed (i.i.d.) uniform random variables. The variable p can vary from 0 to 1 and intuitively the process becomes more irregular as p increases [32]. MIX(p) is defined as [32]

$$\mathrm{MIX}(p)_j = (1 - z_j)x_j + z_j y_j, \tag{10}$$

where $x_j = \sqrt{2} \times \sin(\frac{2\pi j}{12})$ for all j, and y_j = i.i.d. uniform random variables on $[-\sqrt{3}, \sqrt{3}]$. z_j is a binary variable where $z_j = 1$ with probability p and $z_j = 0$ with probability $1-p$. The appellation MIX indicates that the process is a mixture of deterministic and stochastic components. For the 2D case, we use the $\mathrm{MIX_{2D}}(p)$ process [22]. The latter is based on the one-dimensional definition [22]

$$\mathrm{MIX}_{2D}(p)_{i,j} = (1 - z_{i,j})x_{i,j} + z_{i,j}y_{i,j}, \tag{11}$$

where $x_{i,j} = \sin(\frac{2\pi i}{12}) + \sin(\frac{2\pi j}{12})$ is a sinusoidal image, and $\mathbf{Y} = \{y_{i,j}\}$ is an image containing uniform white noise in the range $[-\sqrt{3}, \sqrt{3}]$. $z_{i,j} = 1$ with probability p and $z_{i,j} = 0$ with probability $1 - p$. Depending on the p value, the resulting image presents a specific degree of spatial regularity: when $p = 1$, $\mathrm{MIX_{2D}}(p)$ is a purely random function (highly irregular image); when $p = 0$, we obtain a bi-dimensional sine function (a perfectly regular periodic image), as it is the case for the one-dimensional case; see examples of such images in Figure 3. In our work, various realizations of $\mathrm{MIX_{2D}}$ images

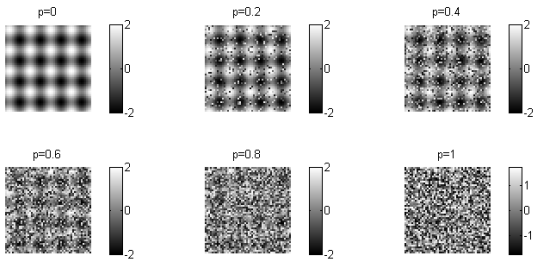

Figure 3: Examples of $\mathrm{MIX}_{2\mathrm{D}}$ images for different p values.

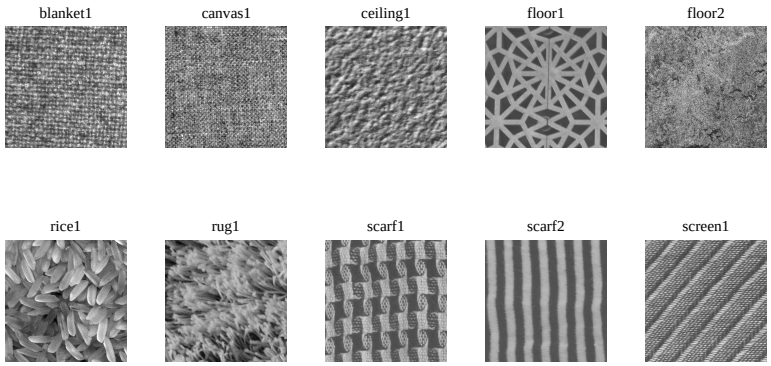

Figure 4: One sample of each of the ten selected groups from Kylberg textures [31]. All images have a size of 576×576 pixels.

of size 256×256 pixels were generated and analyzed (one $\mathrm{MIX}_{2\mathrm{D}}$ per set of parameter values).

3.2. Real Datasets

3.2.1. Kylberg Texture Dataset

We also used a subset of the Kylberg texture dataset. We selected 10 groups of images, each one includes 1000 samples, representing fabrics and surfaces of rotated images, namely floor1, floor2, scarf1, scarf2, rug1, rice1, screen1, ceiling1, blanket1, and canvas1 [31]. One sample, sized 576×576 pixels, of each of them is depicted in Figure 4. The dataset is publicly available at `http://www.cb.uu.se/~gustaf/texture`. For more information, please refer to [31].

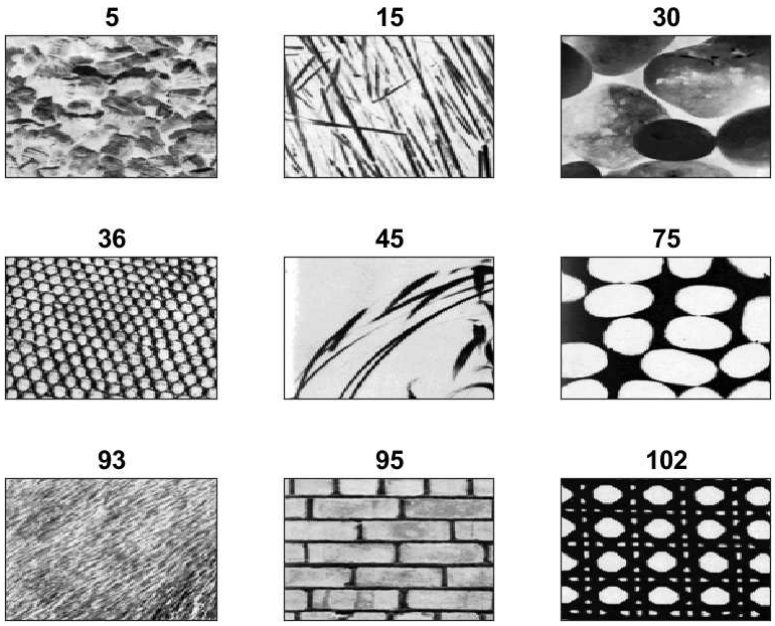

Figure 5: The Brodatz image dataset used. Each image is 128×128 pixels.

3.2.2. Brodatz Image Dataset

The DispEn_{2D} method was also compared with SampEn_{2D} on the Brodatz grayscale texture album [33]. This dataset is composed of 112 grayscale images representing a large variety of natural textures. This album is now widely used in the literature (see, e.g., [34, 35, 36]). From this album we extracted 9 groups of images, as already performed in another study dealing with SampEn_{2D} [22]. From each group, we used one arbitrary sample image sized 128×128 pixels, as shown in Figure 5.

3.2.3. Cardiac Histological Images from Rats

We also evaluated DispEn_{2D} and SampEn_{2D} in a biomedical application. Thus, cardiac histological images from rats were processed. The acquisition procedure is described below.

Myocardial Infarction in Rats:. Fourteen male Wistar rats (280-300 g) were submitted to myocardial infarction (MI group; 8 rats) or sham surgery procedures (SHAM group; 6 rats). Myocardial infarction was produced by a method similar to the one described in [37]. Briefly, the rats were anesthetized with ketamine (50 mg/kg, intraperitoneal) and xilazine (10 mg/kg,

intraperitoneal), endotracheally intubated and mechanically ventilated with room air. A left thoracotomy was performed at the fifth intercostal space and the left anterior descending coronary artery was ligated between the pulmonary artery outflow tract and the left atrium with a polyester suture. The thorax was immediately closed after coronary ligation. Control (SHAM) rats were submitted to the same operative procedures as MI rats with exception of the coronary artery ligation. Experimental protocol was reviewed and approved by the Committee of Ethics in Animal Research of the School of Medicine of Ribeirao Preto, University of Sao Paulo, SP, Brazil (Protocol #165/2016).

Morphological Analysis:. After four weeks of MI or SHAM surgeries, rats were euthanized with an overdose of anesthetic (tribomoethanol, 250 mg/kg, intraperitoneal). The hearts were withdrawn from the thoracic cavity, cut transversely, fixed in phosphate-buffered 10% formalin and submitted to paraffin inclusion for histological study. Sections of 7 μm thick were cut and stained with Masson's trichrome stain to identify and quantify interstitial collagen fibers which plays an important role in the structural organization of the heart. Stained cross-sections were captured using light microscopy (Leica DM5500B; Leica Microsystem, Wetzlar, Germany) at $\times$40 magnification. For each heart, one image from the septum of the left ventricle was selected for posterior analysis.

During images acquisition, it was observed that histological tissue processing was deficient, which resulted in poor quality images. This fact makes this dataset particularly interesting to the present study, creating a scenario where it is possible to evaluate the performance of the two-dimensional entropy measures ($\text{DispEn}_{2\text{D}}$ and $\text{SampEn}_{2\text{D}}$) for the classification of low quality images obtained from different sources, i.e. pathological (MI) and non pathological (SHAM) groups.

All the histological images were originally sized 2048 $\times$ 1536 pixels and RGB-colored. To reduce the computational time, the entire dataset was downsampled to 1024 $\times$ 768 pixels with a linear interpolation and converted to a 8-bit grayscale representation prior to the analyzes. Figure 6 shows one representative image from each group (SHAM and MI).

Comparisons of entropy values between groups in the cardiac histological image dataset were performed with Mann-Whitney rank sum test due to the small sample size. Significance was set at $P < 0.05$.

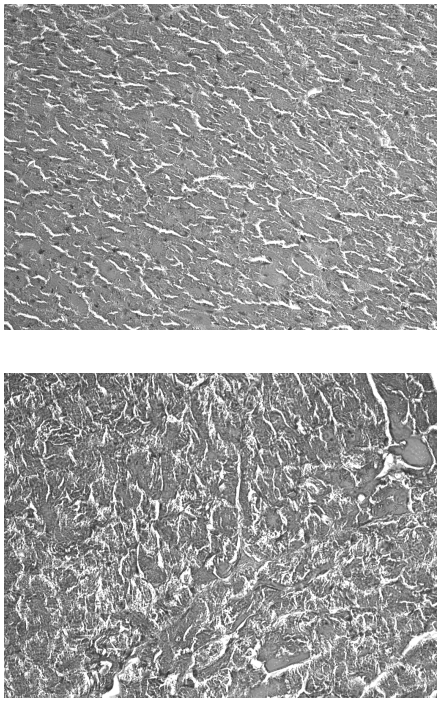

Figure 6: Representative examples of cardiac histological image dataset used in this study, obtained from SHAM (upper image) and myocardial infarction (lower image) groups. All images have a size of 1024×768 pixels.

4. Results and Discussion

In this Section, we assess the ability of $\mathrm{DispEn}_{2\mathrm{D}}$ to characterize different kinds of synthetic and real datasets described in Section 3. Note that for simplicity, we set $\mathbf{m} = [2, 2]$ and $c = 5$ for $\mathrm{DispEn}_{2\mathrm{D}}$ in all simulations below, even though the ranges $3 \leq c \leq 8$ and $[1, 1] \leq [m, m] \leq [5, 5]$ lead to similar findings (data not shown).

4.1. Synthetic Datasets

4.1.1. Texture Image with Additive Noise

The two-dimensional entropy values obtained from the Lenna image with different amounts of $\mathrm{WGN}_{2\mathrm{D}}$ and $\mathrm{SPN}_{2\mathrm{D}}$ are shown in Table 1. They reveal that the addition of $\mathrm{WGN}_{2\mathrm{D}}$ of larger mean and variance leads to higher entropy values for both the $\mathrm{DispEn}_{2\mathrm{D}}$ and $\mathrm{SampEn}_{2\mathrm{D}}$ methods. There is an overlap between the $\mathrm{SampEn}_{2\mathrm{D}}$ values with mean and variance 0.05 and

Table 1: Mean value and standard deviation (40 realizations) of DispEn_{2D} and SampEn_{2D} computed from the reference image (Lenna, Figure 1) on which different levels of bi-dimensional white Gaussian noise (WGN_{2D}) and salt and pepper noise (SPN_{2D}) were added. We used $\mathbf{m} = [2, 2]$ for and $c = 5$ for DispEn_{2D}. The parameters were set to $\mathbf{m} = [2, 2]$ for both the methods, $c = 5$ for DispEn_{2D} and $r = 0.24$ of image standard deviation for SampEn_{2D}.

Type of noise	Level added	DispEn_{2D}	SampEn_{2D}
WGN_{2D}	mean and variance 0.01	5.0555±0.0074	6.5653±0.0204
WGN_{2D}	mean and variance 0.05	5.9766±0.0075	8.1864±0.0567
WGN_{2D}	mean and variance 0.09	6.1006±0.0049	8.2703±0.1020
SPN_{2D}	density 0.01	3.2805±0.0045	0.7715±0.0057
SPN_{2D}	density 0.05	3.6846±0.0100	1.1095±0.0146
SPN_{2D}	density 0.09	4.0077±0.0107	1.4911±0.0229

those for mean and variance 0.09. However, there is no overlap between any two groups for DispEn_{2D}, demonstrating its advantage over SampEn_{2D}.

Likewise, adding SPN_{2D} with larger noise density results in higher entropy values. Both evidence that DispEn_{2D} can detect different levels of WGN_{2D} and SPN_{2D}, where the greater the amount of noise, the higher the DispEn_{2D} value. For SPN with density d, the noise is applied to d multiplied by the number of pixels of an image. However, for the WGN case, the noise is added to almost every pixel of an image. Thus, the DispEn_{2D} and SampEn_{2D} values for WGN, compared with their counterparts for SPN, are larger. It is worth noting that the results for various images lead to similar findings as well (for briefness reasons, we do not show them here).

4.1.2. Artificial Periodic and Synthesized Textures

Table 2 shows that the DispEn_{2D}, like SampEn_{2D}, of a periodic texture image is lower than that of its corresponding synthesized one. This fact suggests that DispEn_{2D} and SampEn_{2D} can be considered as metrics to quantify the regularity or predictability of images.

4.1.3. Two-dimensional MIX Process (MIX_{2D})

Figure 7 shows the entropy of MIX_{2D} process using DispEn_{2D} ($c = 5$) and SampEn_{2D} ($r = 0.24$) for $\mathbf{m} = \{[1, 1], [2, 2], [3, 3]\}$. The parameters used for SampEn_{2D} were chosen according to [22]. The MIX_{2D} process goes from the absolutely regular ($p = 0$) to the completely random ($p = 1$) and one expects

Table 2: DispEn_{2D} and SampEn_{2D} of (a), (b), (c), and (d) periodic textures and their (e), (f), (g), and (h) synthesized corresponding textures; see Figure 2. The parameters were set to $\mathbf{m} = [2, 2]$ for both the methods, $c = 5$ for DispEn_{2D} and $r = 0.24$ of image standard deviation for SampEn_{2D}.

	Texture (a)	Texture (b)	Texture (c)	Texture (d)
DispEn_{2D}	1.018	1.110	2.445	4.124
	Texture (e)	Texture (f)	Texture (g)	Texture (h)
DispEn_{2D}	1.088	1.203	2.664	4.305
	Texture (a)	Texture (b)	Texture (c)	Texture (d)
SampEn_{2D}	0.0885	0.1818	0.1647	0.1187
	Texture (e)	Texture (f)	Texture (g)	Texture (h)
SampEn_{2D}	0.1025	0.1827	0.3123	0.1310

entropy to increase for increasing p. This is the case for both evaluated measurements, except for DispEn_{2D} with $\mathbf{m} = [1, 1]$. Since dispersion patterns should have at least two elements, the embedding dimension for DispEn_{2D} has to be set at least to $[2, 2]$. For this reason, the DispEn_{2D} values for $\mathbf{m} = [1, 1]$ are almost constant. According to Gonzalez [38], "a pattern is essentially an arrangement and it is characterized by the order of the elements of which it is made". Thus, it is highly recommended to have at least two elements in a pattern, as suggested to set $m > 1$ for DispEn_{1D} [7, 13]. The reason behind the constant value is that $\ln(c^{m_h \times m_w}) = \ln(5) = 1.6094$ is the maximum DispEn_{2D} value for $m = [1, 1]$. In addition, SampEn_{2D} for $\mathbf{m} = [3, 3]$ and $p = 0.5$ shows instability. The curve for SampEn_{2D} with $\mathbf{m} = [3, 3]$ is not a monotonic increase for $p > 0.5$ and there is a missing value at $p = 0.95$. This is explained by the fact that patterns become harder to find in SampEn_{2D} as $\mathbf{m}$ increases [22]. Therefore, SampEn_{2D} becomes poorly estimated for increasing $\mathbf{m}$, especially for small images.

4.2. Real Datasets

4.2.1. Kylberg Texture Dataset

To assess the ability of DispEn_{2D} to be used as a feature extraction method for images or textures, we used the popular publicly-available Kylberg Texture Dataset. The DispEn_{2D} values for the selected Kylberg texture groups are demonstrated in Table 3. The results illustrate that there are no overlaps between entropy values of the ten selected groups, showing that DispEn_{2D} may be a useful metric to distinguish different patterns of fabrics and sur-

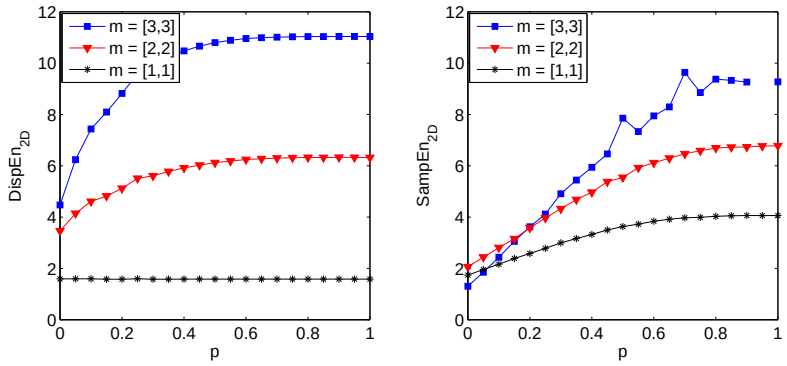

Figure 7: DispEn_{2D} (left panel) and SampEn_{2D} (right panel) calculated from MIX_{2D} processes of size 256×256 pixels. The parameters were set to $\mathbf{m} = \{[1,1],[2,2],[3,3]\}$ for both the methods, $c = 5$ for DispEn_{2D} and $r = 0.24$ of image standard deviation for SampEn_{2D}.

faces.

Table 3: $\mathrm{DispEn}_{2\mathrm{D}}$ of ten different groups of textured surfaces shown as mean ± standard deviation; see Figure 4. The values $\mathbf{m} = [2, 2]$ and $c = 5$ were chosen for the computation.

scarf2	floor1	scarf1	rug1	rice1	screen1	ceiling1	blanket1	canvas1	floor2
2.0550±0.1283	2.5172±0.0678	2.9513±0.1422	3.2192±0.0950	3.5568±0.1438	3.8459±0.0671	4.0812±0.1335	4.6118±0.1042	4.9069±0.0853	5.6082±0.1394

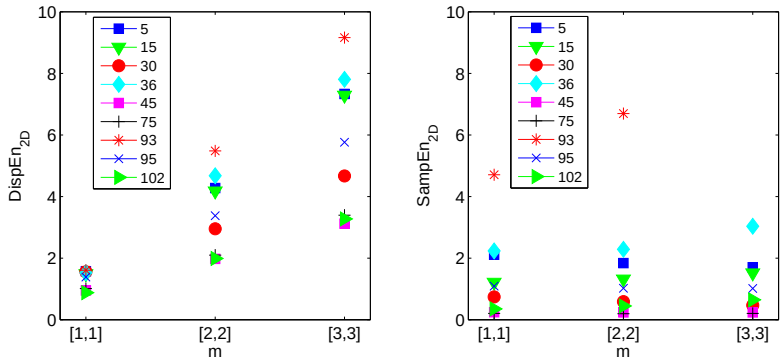

Figure 8: DispEn_{2D} (left panel) and SampEn_{2D} (right panel) calculated from the Brodatz dataset presented in Figure 5. The parameters were set to $\mathbf{m} = \{[1,1],[2,2],[3,3]\}$ for both methods, $c = 5$ for DispEn_{2D} and $r = 0.24$ of image standard deviation for SampEn_{2D}. For SampEn_{2D} and data 93 at $\mathbf{m} = [3,3]$ the computation leads to infinite value.

4.2.2. Brodatz Image Dataset

Results for the Brodatz dataset are depicted in Figure 8. The parameters values for both the entropy approaches are equal to those previously used, i.e. $c = 5$ (DispEn_{2D}) and $r = 0.24$ of image standard deviation (SampEn_{2D}). Interestingly, the orders of the entropy values obtained by DispEn_{2D} and SampEn_{2D} of the images are quite similar. The difference between DispEn_{2D} and SampEn_{2D} was found only for the orders assigned with the three lowest entropy values. Moreover, both measurements show relative consistency. Relative consistency implies that, if $\mathrm{SampEn}_{2D}(m1, r1)(S) > \mathrm{SampEn}_{2D}(m1, r1)(T)$, then $\mathrm{SampEn}_{2D}(m_2, r_2)(S) > \mathrm{SampEn}_{2D}(m_2, r_2)(T)$. Likewise, if $\mathrm{DispEn}_{2D}(m_1, c_1)(S) > \mathrm{DispEn}_{2D}(m_1, c_1)(T)$, then $\mathrm{DispEn}_{2D}(m_2, c_2)(S) > \mathrm{DispEn}_{2D}(m_2, c_2)(T)$ [3].

It is worth pointing out that DispEn_{2D} and SampEn_{2D} are based on different concept in entropy. While SampEn_{2D} is a conditional entropy, i.e. estimates the conditional probability that similar $\mathbf{m}$-size patterns will still be similar for $\mathbf{m} + 1$, DispEn_{2D} is based on the definition of Shannon's entropy, and takes into account only the matches of patterns of size $\mathbf{m}$. The inconsistencies found for DispEn_{2D} for $\mathbf{m} = [1,1]$ might be the result of the entropy estimation method, which is based only on the single pixels distributions, whereas SampEn_{2D}, even for $\mathbf{m} = [1,1]$, takes into account some information on patterns with $\mathbf{m} = [2,2]$.

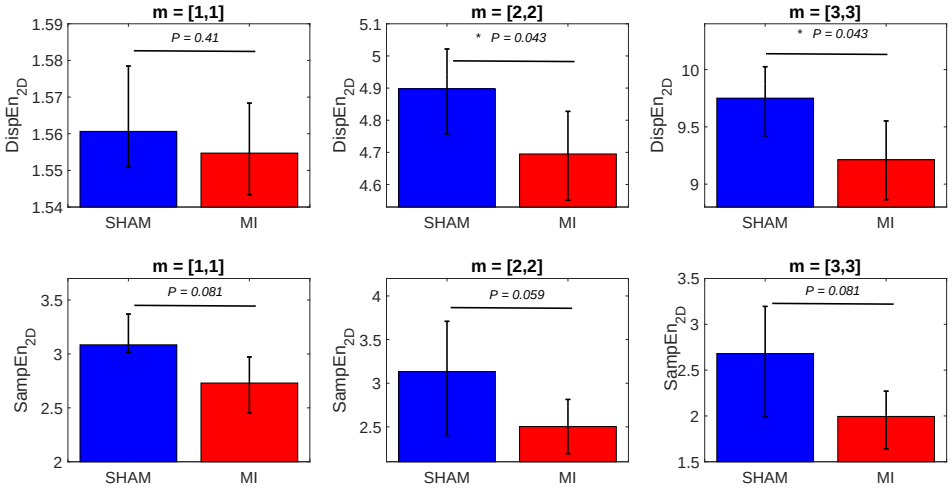

Figure 9: DispEn_{2D} (top panels) and SampEn_{2D} (bottom panels) calculated from the cardiac histological images from rats. The median value of the entropy for each group is presented here, as well as the 25^{th} and 75^{th} percentiles. $*$ means $P < 0.05$. Parameters were set to $\mathbf{m} = \{[1,1],[2,2],[3,3]\}$ for both methods, $c = 5$ for DispEn_{2D} and $r = 0.24$ of image standard deviation for SampEn_{2D}.

4.2.3. Cardiac Histological Images from Rats

The results obtained by DispEn_{2D} and SampEn_{2D} for the cardiac histological image dataset are depicted in Figure 9. In general, the pixel patterns of cardiac fibers from SHAM animals present more irregularity (higher entropy) when compared to MI animals. The SampEn_{2D} of the SHAM animals presented a tendency to higher values compared to the MI, although no statistical significance was found for $\mathbf{m} = [1,1]$, $\mathbf{m} = [2,2]$, or $\mathbf{m} = [3,3]$. DispEn_{2D} led to higher values for the SHAM compared to the MI for $\mathbf{m} = [2,2]$ and $\mathbf{m} = [3,3]$. The lack of difference for $\mathbf{m} = [1,1]$ is not surprising as $\mathbf{m} = [1,1]$ was identified not to be a good choice for DispEn_{2D}. Therefore, we can say that DispEn_{2D} is a valuable measurement to distinguish the SHAM to MI. Even though the DispEn_{2D} curves of the SHAM and MI are closer compared to the respective SampEn_{2D} curves, one must be aware that DispEn_{2D} has a much lower standard deviation (or CV, see Tables 5 and 6). Therefore, the scaling of DispEn_{2D} and SampEn_{2D} are different and must not be directly compared.

The Hedges' g effect size [40] was also employed to quantify the differences

Table 4: Differences between the DispEn_{2D} and SampEn_{2D} results for the cardiac histological images from SHAM vs. MI rats based on the Hedges' g effect size.

Method	$m = [1, 1]$	$m = [2, 2]$	$m = [3, 3]$
DispEn_{2D}	0.6667	1.1896	1.3015
SampEn_{2D}	1	1.1836	1.2051

between the results for SHAM vs. MI. The Hedges' g test shows the difference between the means of two groups, divided by the weighted average of standard deviations for these two groups. The differences, illustrated in Table 4, show that the highest effect size is obtained by DispEn_{2D} with $m = [3, 3]$, suggesting the advantage of this method over SampEn_{2D}.

Results with the cardiac histological dataset give strength to the assumption that irregularity may be a valuable source of information to distinguish the dynamics of images [22]. Even if the present dataset includes low quality images, DispEn_{2D} was able to differentiate pathological from non pathological conditions. This opens new possibilities for application of two-dimensional entropy measurements, even for noisy and corrupted images.

4.3. Sensitivity of DispEn_{2D} and SampEn_{2D} to Image Sizes

To evaluate the sensitivity of DispEn_{2D} and SampEn_{2D} to the size of images, we created 40 different WGN_{2D} and 40 $\text{MIX}_{2D}(0.5)$ with sizes varying from 10×10 to 200×200 pixels. The Parameters c and r were respectively 5 and 0.24 of the standard deviation of images and $\mathbf{m}$ varied in $\{[1, 1], [2, 2], [3, 3]\}$. The mean and standard deviation values of the results for WGN_{2D} and $\text{MIX}_{2D}(0.5)$ are shown in Figure 10.

As mentioned before, SampEn_{2D} counts element pairs in template matrices having $d[\mathbf{X}_{k,l}^{\mathbf{m},\,\mathbf{d}}, \mathbf{X}_{a,b}^{\mathbf{m},\mathbf{d}}] \leq r$. In case the size of an image is small, the probability for this number of being equal to zero is higher, leading to undefined values. Accordingly, the entropy values for small-sized images using SampEn_{2D} with $\mathbf{m} = [2, 2]$ and all values for SampEn_{2D} with $\mathbf{m} = [3, 3]$ are undefined, as can be seen in Figure 10. In contrast, the DispEn_{2D}-based values are always defined, showing an advantage of DispEn_{2D} over SampEn_{2D}.

As mentioned previously, to obtain reliable statistics to calculate DispEn_{2D}, the number of patterns in an image, i.e. $(h - (m_h - 1)) \times (w - (m_w - 1))$, has to be greater than the number of potential patterns ($c^{m_h \times m_w}$). In Figure 10, for $\mathbf{m} = [2, 2]$ and for image sizes varying from 40×40 to 200×200 pixels, we

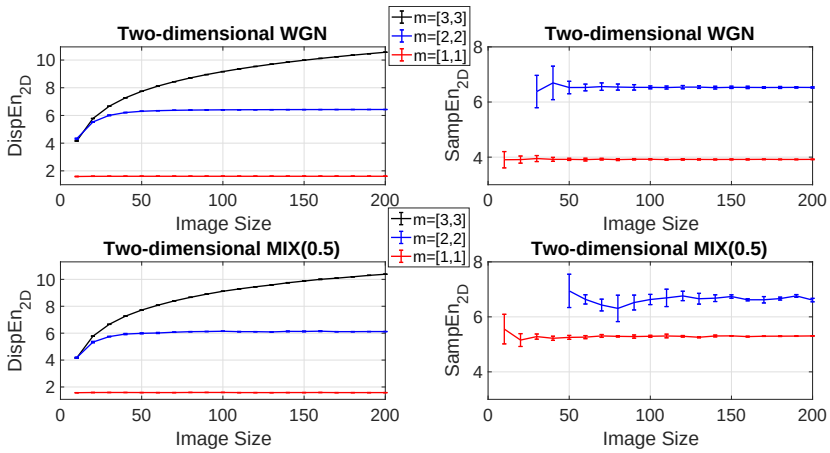

Figure 10: Mean and standard deviation for DispEn_{2D} ($c = 5$) and SampEn_{2D} ($r = 0.24\times$ standard deviation of the image) with embedding dimensions [1,1], [2,2], and [3,3] as functions of image size changing from 10×10 to 200×200 pixels computed from 40 different WGN_{2D} and $\text{MIX}_{2D}(0.5)$. SampEn_{2D} values for image sizes of 10×10 pixels and 20×20 pixels with $\mathbf{m} = [2, 2]$ and all SampEn_{2D} values for $\mathbf{m} = [3, 3]$ are undefined.

have between 1521 and 39601 patterns in the images, respectively, with 625 potential patterns defined in DispEn_{2D}. The statistics obtained can therefore be considered as reliable. However, for $\mathbf{m} = [3, 3]$, we have between 1444 (for an image size of 40×40 pixels) and 39204 (for an image size of 200×200 pixels) patterns in the images, with 1953125 potential patterns in DispEn_{2D}. The number of potential dispersion patterns is therefore much larger than the number of patterns extracted from the image. This explains why DispEn_{2D} values for $\mathbf{m} = [3, 3]$ shows a different behavior for image sizes larger than 40×40 pixels. The maximum DispEn_{2D} value is $\ln(c^{m_h \times m_w})$. For $c = 5$ and $\mathbf{m} = [2, 2]$ this gives a maximum entropy value of 6.43 (value nearly observed in Figure 10 for $\mathbf{m} = [2, 2]$ and image sizes larger than 40×40 pixels). For $c = 5$ and $\mathbf{m} = [3, 3]$, the maximum entropy value is 14.48. For $c = 5$ and $\mathbf{m} = [3, 3]$, we may need images larger than 1400×1400 pixels to reach this maximum value.

To compare the stability of the results obtained by DispEn_{2D} and SampEn_{2D}, we used the coefficient of variation (CV) defined as the standard deviation divided by the mean. The CV permits comparison of variability estimates regardless of the magnitude values [39]. The CV values of the results for sizes 50×50, 100×100, 150×150, and 200×200 pixels using WGN_{2D} and $\text{MIX}_{2D}(0.5)$ are shown in Tables 5 and 6, respectively. Forty realizations

Table 5: Coefficient of variation (CV) values for the DispEn_{2D} and SampEn_{2D} for different sizes of WGN_{2D} for 40 realizations of each size. r and c were respectively 0.24 of the standard deviation of images and 5.

Methods	50×50	100×100	150×150	200×200
DispEn_{2D} with $\mathbf{m}=[1,1]$	23e-05	4e-05	2e-05	1e-05
DispEn_{2D} with $\mathbf{m}=[2,2]$	140e-05	32e-05	12e-05	6e-05
DispEn_{2D} with $\mathbf{m}=[3,3]$	9.9535e-05	6e-05	6e-05	6e-05
SampEn_{2D} with $\mathbf{m}=[1,1]$	990e-05	5000e-05	420e-05	280e-05
SampEn_{2D} with $\mathbf{m}=[2,2]$	3460e-05	790e-05	630e-05	340e-05
SampEn_{2D} with $\mathbf{m}=[3,3]$	undefined	undefined	undefined	undefined

Table 6: Coefficient of variation (CV) values for the DispEn_{2D} and SampEn_{2D} for different sizes of $\text{MIX}_{2D}(p=0.5)$ (40 realizations of each size). r and c were respectively 0.24 of the standard deviation of images and 5.

Methods	50×50	100×100	150×150	200×200
DispEn_{2D} with $\mathbf{m}=[1,1]$	0.0021	0.0007	0.0026	0.0008
DispEn_{2D} with $\mathbf{m}=[2,2]$	0.0054	0.0017	0.0043	0.0012
DispEn_{2D} with $\mathbf{m}=[3,3]$	0.0011	0.0004	0.0017	0.0004
SampEn_{2D} with $\mathbf{m}=[1,1]$	0.0872	0.0280	0.0091	0.0094
SampEn_{2D} with $\mathbf{m}=[2,2]$	0.0135	0.0066	0.0014	0.0008
SampEn_{2D} with $\mathbf{m}=[3,3]$	undefined	undefined	undefined	undefined

of each type of synthetic image were used. DispEn_{2D} ($c=5$) and SampEn_{2D} ($r=0.24$ of images standard deviation) were calculated for different values of $\mathbf{m}$. Generally, for WGN_{2D}, the larger the image size, the smaller the CV value for both DispEn_{2D} and SampEn_{2D}. For both WGN_{2D} and $\text{MIX}_{2D}(0.5)$, the CV values obtained with DispEn_{2D} are noticeably smaller than those obtained with SampEn_{2D}. Moreover, the CVs for SampEn_{2D} with $\mathbf{m}=[3,3]$ are undefined.

4.4. Computational Time

Figure 11 shows the computational time (in seconds) to calculate DispEn_{2D} and SampEn_{2D} in the Brodatz dataset, as a function of c or r, and different values of $\mathbf{m}$. The time to compute DispEn_{2D} increases exponentially with c and is very sensitive to $\mathbf{m}$. In contrast, the computational time of SampEn_{2D} increases linearly with r and is much less sensitive to $\mathbf{m}$. However, the time required to calculate DispEn_{2D} is markedly lower than the

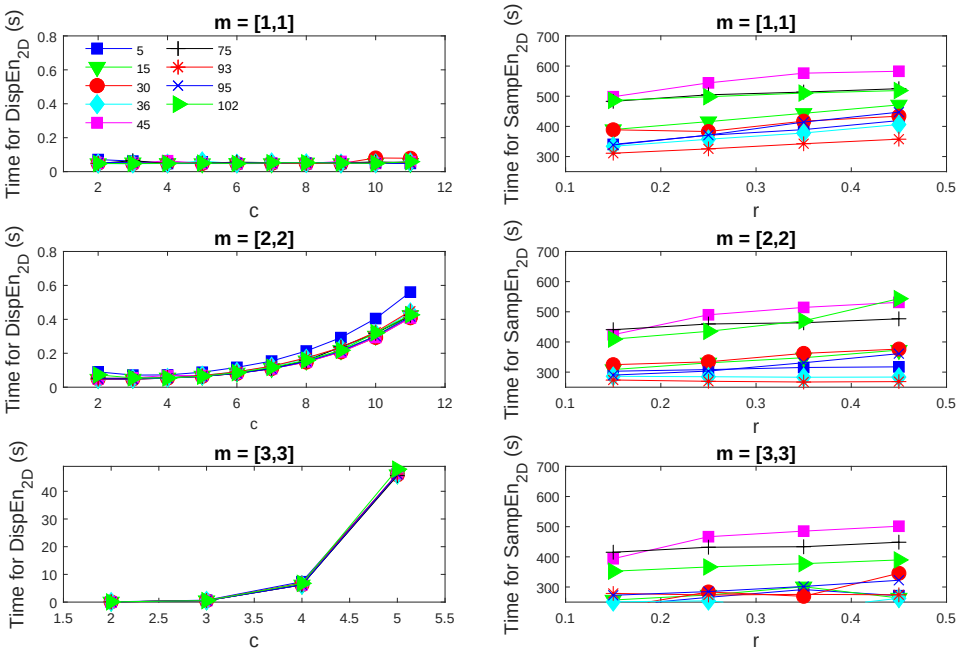

Figure 11: Computational time for $\mathrm{DispEn_{2D}}$ (left panels) and $\mathrm{SampEn_{2D}}$ (right panels) calculated using the Brodatz dataset (images sized 128×128 pixels), for different values of parameters $\mathbf{m}$, c and r.

time required to compute $\mathrm{SampEn_{2D}}$. In the conditions of Figure 8, in case $\mathbf{m} = [3, 3]$, the computation of $\mathrm{DispEn_{2D}}$ ($c = 5$) takes around 45 s, whereas that of $\mathrm{SampEn_{2D}}$ ($r = 0.24$) takes from roughly 250 to 500 s (approximately 8 times higher computational time). The computational time is an important limitation of $\mathrm{SampEn_{2D}}$ that $\mathrm{DispEn_{2D}}$ notably outperforms. Moreover, Figure 11 shows that there is no major difference in the computational times using $\mathrm{DispEn_{2D}}$ for different images. However, in $\mathrm{SampEn_{2D}}$, because there is a difference in the number of patterns considered as similar in each image, the computational time depends on the image processed.

$\mathrm{DispEn_{2D}}$ and $\mathrm{SampEn_{2D}}$ have the following advantages as image processing tools: 1) they are entropy measurements that take into account the spatial properties of pixels; 2) they are not very sensitive to noise; and 3) they are insensitive to translation and rotation. $\mathrm{DispEn_{2D}}$ and $\mathrm{SampEn_{2D}}$ may be helpful in several applications of image processing field, such as pat-

tern recognition, segmentation and event detection, considering that the one-dimensional version of those methods have been successfully applied in such problems [41, 42]. $\text{DispEn}_{2\text{D}}$ is much faster than $\text{SampEn}_{2\text{D}}$ and will never return an undefined entropy value.

We have very recently introduced the bi-dimensional distribution entropy ($\text{DistrEn}_{2\text{D}}$) for small-sized images [27]. In spite of its interesting results, as can be seen in Table 5 in [27] compared with Figure 11, $\text{DispEn}_{2\text{D}}$ is considerably faster than $\text{DistrEn}_{2\text{D}}$. Additionally, as the total number of elements in distance matrix $\mathbf{D}$ is about h^2w^2, the computation of $\text{DistrEn}_{2\text{D}}$ for large-sized images requires the storage of a huge number of elements. It is one reason that we stressed the importance of $\text{DistrEn}_{2\text{D}}$ for only small-sized textures [27], whereas $\text{DispEn}_{2\text{D}}$ can take into account both small and large images. More importantly, according to the $\text{DistrEn}_{2\text{D}}$ algorithm, new images created simply by random permutations of an original image have $\text{DistrEn}_{2\text{D}}$ values close to the original image. For instance, if the elements of $\text{MIX}_{2\text{D}}(0.5)$ are sorted, its $\text{DistrEn}_{2\text{D}}$ value is not changed considerably. However, as expected theoretically, sorting leads to a lower entropy value.

5. Conclusion

The aim of this study was to develop $\text{DispEn}_{2\text{D}}$ based on Shannon's definition of entropy and the recently introduced dispersion patterns to quantify the irregularity or uncertainty of images. We evaluated the $\text{DispEn}_{2\text{D}}$ method on synthetic and real datasets. The study done here has the following implications for the estimation of images' irregularity. First, $\text{DispEn}_{2\text{D}}$ distinguished different amounts of $\text{WGN}_{2\text{D}}$ and $\text{SPN}_{2\text{D}}$ and discriminated the periodic images from their corresponding synthesized ones. Moreover, $\text{DispEn}_{2\text{D}}$ was found to be a powerful feature extraction method to detect the patterns of images from different kinds of Kylberg textures. Furthermore, $\text{DispEn}_{2\text{D}}$ detected different degrees of irregularity of $\text{MIX}_{2\text{D}}$. Also, the results from the Brodatz dataset showed the stability of $\text{DispEn}_{2\text{D}}$-based results. In addition, $\text{DispEn}_{2\text{D}}$, unlike $\text{SampEn}_{2\text{D}}$, significantly discriminated the pathological from non pathological conditions in a dataset composed of low quality images. Finally, $\text{DispEn}_{2\text{D}}$ has three key advantages over $\text{SampEn}_{2\text{D}}$: 1) $\text{DispEn}_{2\text{D}}$, unlike $\text{SampEn}_{2\text{D}}$, does not result in undefined values; 2) $\text{DispEn}_{2\text{D}}$ is noticeably faster; and 3) $\text{DispEn}_{2\text{D}}$-based values are noticeably more stable than those obtained by $\text{SampEn}_{2\text{D}}$ based on the coefficient of variation test.

Overall, due to its ability to detect different kinds of dynamics of images, DispEn_{2D} has a great potential to analyze various images with low computational time.

References

[1] R. C. Gonzalez and R. E. Woods, "Image processing", *Digital Image Processing*, vol. 2, 2007.

[2] C. E. Shannon, "A mathematical theory of communication," *ACM SIGMOBILE Mobile Computing and Communications Review*, vol. 5, no. 1, pp. 3–55, 2001.

[3] J. S. Richman and J. R. Moorman, "Physiological time-series analysis using approximate entropy and sample entropy," *American Journal of Physiology-Heart and Circulatory Physiology*, vol. 278, no. 6, pp. H2039–H2049, 2000.

[4] S. M. Pincus, "Approximate entropy as a measure of system complexity," *Proceedings of the National Academy of Sciences*, vol. 88, no. 6, pp. 2297–2301, 1991.

[5] C. Bandt and B. Pompe, "Permutation entropy: a natural complexity measure for time series," *Physical Review Letters*, vol. 88, no. 17, p. 174102, 2002.

[6] P. Li, C. Liu, K. Li, D. Zheng, C. Liu, and Y. Hou, "Assessing the complexity of short-term heartbeat interval series by distribution entropy", *Medical and Biological Engineering and Computing*, vol. 53, pp. 77–87, 2015.

[7] M. Rostaghi and H. Azami, "Dispersion entropy: A measure for time series analysis", *IEEE Signal Processing Letters*, vol. 23, no. 5, pp. 610–614, 2016.

[8] M. M. Platisa and V. Gal, "Dependence of heart rate variability on heart period in disease and aging", *Physiological Measurement*, vol. 27, no. 10, p. 989, 2006.

[9] D. Abásolo, R. Hornero, P. Espino, D. Alvarez, and J. Poza, "Entropy analysis of the EEG background activity in Alzheimer's disease patients", *Physiological Measurement*, vol. 27, no. 3, p. 241, 2006.

[10] M. O. Sokunbi, "Sample entropy reveals high discriminative power between young and elderly adults in short fMRI data sets", *Information-based Methods for Neuroimaging: Analyzing Structure, Function and Dynamics*, vol. 8, pp. 1–12, 2015.

[11] A. Humeau, F. Chapeau-Blondeau, D. Rousseau, P. Rousseau, W. Trzepizur, and P. Abraham, "Multifractality, sample entropy, and wavelet analyses for age-related changes in the peripheral cardiovascular system: Preliminary results", *Medical Physics*, vol. 35, no. 2, pp. 717–723, 2008.

[12] M. Zanin, L. Zunino, O. A. Rosso, and D. Papo, "Permutation entropy and its main biomedical and econophysics applications: a review", *Entropy*, vol. 14, no. 8, pp. 1553–1577, 2012.

[13] H. Azami and J. Escudero, "Amplitude-and fluctuation-based dispersion entropy", *Entropy*, vol. 20, no. 3, article id. 210, 2018.

[14] S. Tufféry, Data mining and statistics for decision making (Vol. 2). Chichester: Wiley, 2011.

[15] G. Baranwal and D. P. Vidyarthi, "Admission control in cloud computing using game theory", *The Journal of Supercomputing*, vol. 72(1), pp. 317-346, 2016.

[16] M. N. Gibbs and D. J. MacKay, "Variational Gaussian process classifiers", *IEEE Transactions on Neural Networks*, vol. 11(6), pp. 1458-1464, 2000.

[17] W. Duch, "Uncertainty of data, fuzzy membership functions, and multilayer perceptrons", *IEEE Transactions on Neural Networks*, vol. 16(1), pp. 10-23, 2005.

[18] T. Marchant, M. Murphy, G. Madden, and C. Moore, "Quantifying structure regularity in fluorescence microscopy cell images using a novel multi-dimensional approximate entropy metric", in *Image Processing*

(ICIP), 2011 18th IEEE International Conference on, pp. 3085–3088, IEEE, 2011.

[19] C. J. Moore, "A threshold structure metric for medical image interrogation: The 2D extension of approximate entropy", in *Information Visualisation (IV), 2016 20th International Conference*, pp. 336–341, 2016.

[20] C. Moore and T. Marchant, "The approximate entropy concept extended to three dimensions for calibrated, single parameter structural complexity interrogation of volumetric images", *Physics in Medicine and Biology*, vol. 62 pp. 6092–6107, 2017.

[21] L. E. V. da Silva, A. C. da Silva Senra Filho, V. P. S. Fazan, J. C. Felipe, and L. O. Murta, "Two-dimensional sample entropy analysis of rat sural nerve aging", *Engineering in Medicine and Biology Society (EMBC), 36th Annual International Conference of the IEEE*, pp. 3345–3348, 2014.

[22] L. Silva, A. Senra Filho, V. Fazan, J. Felipe, and L. M. Junior, "Two-dimensional sample entropy: assessing image texture through irregularity", *Biomedical Physics & Engineering Express*, vol. 2, no. 4, p. 045002, 2016.

[23] H. V. Ribeiro, L. Zunino, E. K. Lenzi, P. A. Santoro, and R. S. Mendes, "Complexity-entropy causality plane as a complexity measure for two-dimensional patterns", *PLoS ONE*, vol. 7, no. 8, p. e40689, 2012.

[24] L. Zunino and H. V. Ribeiro, "Discriminating image textures with the multiscale two-dimensional complexity-entropy causality plane", *Chaos, Solitons & Fractals*, vol. 91, pp. 679-688, 2016.

[25] H. Y. Sigaki, M. Perc, and H. V. Ribeiro, "History of art paintings through the lens of entropy and complexity", *Proceedings of the National Academy of Sciences*, vol. 115(37), pp. E8585-E8594, 2018.

[26] S. D. Wu, C. W. Wu, and A. Humeau-Heurtier, "Refined scale-dependent permutation entropy to analyze systems complexity," *Physica A: Statistical Mechanics and its Applications*, vol. 450, pp. 454-461, 2016.

[27] H. Azami, J. Escudero, and A. Humeau-Heurtier, "Bidimensional distribution entropy to analyze the irregularity of small-sized textures", *IEEE Signal Processing Letters*, vol. 24, pp. 1338–1342, 2017.

[28] L. E. Silva, J. J. Duque, J. C. Felipe, L. O. Murta Jr, A. Humeau-Heurtier, "Two-dimensional multiscale entropy analysis: Applications to image texture evaluation", *Signal Processing*, vol. 147, pp. 224–232, 2018.

[29] `https://graphics.stanford.edu/projects/texture/demo/synthesis_eero.html`.

[30] L. Y. Wei and M. Levoy, Fast texture synthesis using tree-structured vector quantization. In Proceedings of the 27th annual conference on Computer graphics and interactive techniques (pp. 479-488). ACM Press/Addison-Wesley Publishing Co., (2000, July).

[31] G. Kylberg, *Kylberg Texture Dataset v. 1.0.* Centre for Image Analysis, Swedish University of Agricultural Sciences and Uppsala University, 2011.

[32] S. M. Pincus and A. L. Goldberger, "Physiological time-series analysis: what does regularity quantify?", *American Journal of Physiology*, vol. 266, pp. H1643–H1656, 1994.

[33] P. Brodatz, *Textures: a photographic album for artist & designers.* New York, USA: Dover; 1966, 1966.

[34] W. L. Lee and K. S. Hsieh, "A robust algorithm for the fractal dimension of images and its applications to the classification of natural images and ultrasonic liver images", *Signal Processing*, vol. 90, pp. 1894–1904, 2010.

[35] J. B. Florindo and O. M. Bruno, "Fractal descriptors based on Fourier spectrum applied to texture analysis", *Physica A*, vol. 391, pp. 4909–4922, 2012.

[36] R. Davarzani, S. Mozaffari, and K. Yaghmaie, "Scale- and rotation-invariant texture description with improved local binary pattern features", *Signal Processing*, vol. 111, pp. 274–293, 2015.

[37] M. A. Pfeffer, J. M. Pfeffer, M. C. Fishbein, P. J. Fletcher, J. Spadaro, R. A. Kloner, and E. Braunwald, "Myocardial infarct size and ventricular function in rats", *Circulation Research*, vol. 44, pp. 503–512, 1979.

[38] R. C. Gonzalez, Object Recognition, in Digital image processing, 3rd ed. Pearson, August 2008, pp. 861-909.

[39] G. F. Reed, F. Lynn, and B. D. Meade, "Use of coefficient of variation in assessing variability of quantitative assays," *Clinical and Vaccine Immunology*, vol. 9, no. 6, pp. 1235–1239, 2002.

[40] R. Rosenthal, H. Cooper, and L. Hedges, "Parametric measures of effect size," *The Handbook of Research Synthesis*, vol. 621, pp. 231–244, 1994.

[41] P. Micó, M. Mora, D. Cuesta-Frau, and M. Aboy, "Automatic segmentation of long-term ecg signals corrupted with broadband noise based on sample entropy", *Computer Methods and Programs in Biomedicine*, vol. 98, no. 2, pp. 118–129, 2010.

[42] H. Azami and J. Escudero, "Amplitude-aware permutation entropy: Illustration in spike detection and signal segmentation", *Computer Methods and Programs in Biomedicine*, vol. 128, pp. 40–51, 2016.